J. Fluid Mech. (2007), *vol.* 584, *pp.* 157–183.
doi:10.1017/S0022112007006350 Printed in the United Kingdom

Stability of an evaporating thin liquid film

OLEG E. SHKLYAEV AND ELIOT FRIED

Department of Mechanical & Aerospace Engineering Washington University in St Louis, Campus Box 1185 St Louis, MO 63130-4899, USA

(Received 7 June 2006 and in revised form 2 March 2007)

We use a newly developed set of interface conditions to revisit the problem of an evaporating thin liquid film. In particular, instead of the conventional Hertz–Knudsen–Langmuir equation for the evaporation mass flux, we impose a more general equation expressing the balance of configurational momentum. This balance, which supplements the conventional conditions enforcing the balances of mass, momentum and energy on the film surface, arises from a consideration of configurational forces within a thermodynamical framework. We study the influence of two newly introduced terms on the evolution of the liquid film. One of these terms accounts for the transport of energy within the liquid–vapour interface. The other term, which we refer to as the effective pressure, accounts for vapour recoil. Both new terms are found to be stabilizing. Furthermore, the effective pressure is found to affect a time-dependent base state of the evaporating film and to be an important factor in applications involving liquid films with thicknesses of one or two monolayers. Specifically, we demonstrate that consideration of the effective pressure makes it possible to observe the influence of the van der Waals interactions on film evolution close to the instant of rupture. Dimensional considerations indicate that one of the most significant influences of these effects occurs for molten metals.

1. Introduction

Evaporation is a widespread phenomenon accompanying many physical processes. It plays an important role in the evolution of liquid films. The investigation of liquid films is a rapidly developing field with a wide spectrum of engineering applications (including microfluidics, film deposition, cooling, coating and drying). At present, there are many works devoted to the investigation of different effects helping to predict or control the evolution of liquid films. Relevant problems show rich behaviour and encompass many physical phenomena such as capillarity, thermocapillarity, evaporation and van der Waals interactions. Under certain conditions, each of these effects can substantially influence the evolution of thin films. For a comprehensive review see Oron, Davis & Bankoff 1997.

Deryagin & Churaev (1965) showed that long-range intermolecular forces are capable of initiating flow in a capillary tube and of significantly changing the rate of evaporation. It was recognized that van der Waals forces become important when considering of thin films of thickness less than 1000 Å. Sheludko (1967) showed that, for layer thickness of the order of 100 Å, these forces result in an instability mode and cause the rupture of the film. Criteria for the stability and rupture of a liquid film located on a solid substrate were derived by Jain & Ruckenstein (1976). Later, many works investigated the combined effects of evaporation, capillary and disjoining pressure in liquid systems with curved interfaces. Important examples of such systems

include menisci and constrained vapour bubbles. A detailed review of these works is given by Wayner (1999).

A linear stability analysis of the effect of rapid evaporation on the stability of a liquid–vapour interface was performed by Palmer (1976). By means of linear and nonlinear analyses, Burelbach, Bankoff & Davis (1988) used a single long-wave evolution equation to investigate the influence of effects such as vapour recoil, thermocapillarity, and the disjoining pressure on liquid-film instabilities and rupture. Danov *et al.* (1998) generalized the work of Burelbach *et al.* (1988) to account for the presence of a non-volatile dissolved surfactant. This work discussed the influences of the interfacial viscosity, concentration gradients and Marangoni effects on film stability.

To describe the dynamics of a phase transformation, an additional interface condition accounting for the exchange of material between phases is required. This condition is distinct from, but not inconsistent with, the classical balances for mass, forces, moments and energy. Moreover, it entails the provision of additional constitutive relations. In the literature on evaporation the Hertz–Knudsen–Langmuir equation is commonly used in this capacity. Specifically, the Hertz–Knudsen–Langmuir equation dictates how the deviation between the temperature of the film at the liquid–vapour interface from the saturation temperature drives evaporation or condensation. For a comprehensive discussion of the Hertz–Knudsen–Langmuir equation, see Schrage (1953); for a modern perspective, see Rose (2000). One drawback of the Hertz–Knudsen–Langmuir equation is that its derivation is based on the assumption that the mechanisms underlying evaporation depend only on the states of the liquid and vapour phases, and are independent of mass, momentum and energy transfer (Cammenga 1980). Despite the neglect of these effects, the Hertz–Knudsen–Langmuir equation is, as Koffman, Plesset & Lees (1984) observe, often used without justification in continuum problems involving transfers of mass, momentum and energy.

In this work, we consider the stability of an evaporating liquid film using, instead of the Hertz–Knudsen–Langmuir equation, a more general evaporation boundary condition. That condition arises from a consideration of configurational forces within a thermodynamical framework which explicitly accounts for the mass, momentum and energy transfer across and along the liquid–vapour interface. More importantly, it supplements the conventional conditions enforcing the balances of mass, momentum and energy at the interface. For applications involving solid-state phenomena, the understanding that configurational forces are central to the description of defects has been understood since the studies of Eshelby (1951) and Herring (1951). Gurtin (1988, 1995, 2000) developed a framework wherein these forces obey a configurational momentum balance distinct from and supplemental to the standard (Newtonian) momentum balance. Gurtin's framework generalizes classical interface conditions such as the Gibbs–Thomson equation (Volmer 1939) arising in theories for solidification to situations far from equilibrium where dissipative mechanisms are non-negligible. This idea was exploited by Fried, Gurtin & Shen (2006) to derive a complete set of equations governing the evolution of a sharp interface separating a volatile-solvent/non-volatile-surfactant solution from a vapour atmosphere. Specifically, it was shown that, aside from the classical term involving the difference between the temperatures of the liquid and adjacent vapour at the interface, the interfacial configurational momentum balance accounting for evaporation includes several additional terms. Among these is a term accounting for the combined influence of the capillary and disjoining pressure similar to that considered by Ajaev &

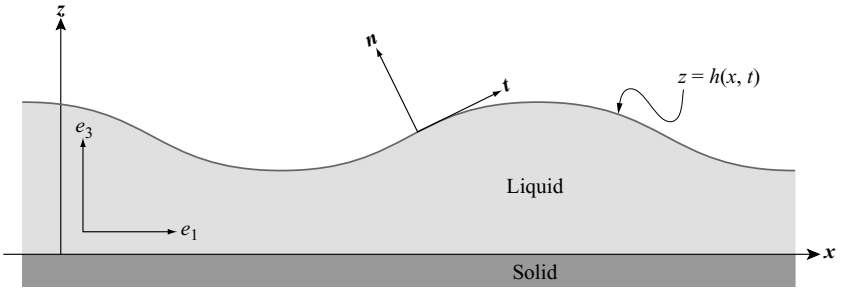

FIGURE 1. Geometry of the system.

Homsy (2001) and Wayner (2002). For brevity, we refer to this as the effective pressure term. We find that a time-dependant base state of evaporating liquid film is tangibly influenced by the effective pressure term. In particular, the effective pressure strongly affects the film rupture processes and is an important factor in the consideration of liquid films with thicknesses of one or two monolayers. These factors lead to a revised understanding of the stability of an evaporating film. Parameter domains where the contributions of the newly introduced terms are important are determined.

The organization of the paper is as follows. In § 2, we formulate the problem and present the governing equations. The time-dependent base state and the influence of the effective pressure on that state are examined in § 3. The effect of different parameters entering the model on the linear stability of the liquid film is presented in § 4. In § 5, we generalize all previous results to account, in the manner of Danov *et al.* (1998), for the presence of a non-volatile dissolved surfactant. Finally, we summarize and briefly discuss our results in § 6. Details of the long-wave approximation applied to derive of the evolution equations are presented in the Appendix.

2. Formulation of the one-sided problem

The system under consideration is a thin film of a viscous incompressible liquid, resting on a horizontal solid substrate (figure 1). The film occupies the region between the solid boundary at $z = 0$ and a free boundary at $z = h(x, t)$. The buoyancy force is neglected and we suppose that the liquid is heated from the solid substrate and evaporates at the free surface.

Following Burelbach *et al.* (1988), we assume that the density $\rho^v > 0$, kinematic viscosity $\nu^v > 0$, and thermal conductivity κ^v of the vapour phase are much smaller than their counterparts ρ, ν and κ in the liquid phase,

$$\rho^v \ll \rho, \qquad \nu^v \ll \nu, \qquad \kappa^v \ll \kappa,$$

so that the use of a one-sided model is justified.

Within the liquid film, the velocity, pressure (of the liquid measured relative to the pressure of vapour), and absolute temperature fields $\boldsymbol{u}$, p, and θ are governed by the

Navier–Stokes, heat conduction and continuity equations:

$$\frac{\mathrm{D}\boldsymbol{u}}{\mathrm{D}t} = -\frac{1}{\rho}\nabla p + \nu\nabla^2\boldsymbol{u}, \tag{2.1a}$$

$$\rho c\frac{\mathrm{D}\theta}{\mathrm{D}t} = \kappa\nabla^2\theta. \tag{2.1b}$$

$$\nabla\cdot\boldsymbol{u} = 0. \tag{2.1c}$$

Here, c denotes the specific heat of the liquid and, as is usual, $\mathrm{D}/\mathrm{D}t$ is the material time derivative and ∇ is the spatial gradient operator.

At the liquid–solid interface $z = 0$, we invoke the no-slip condition for the velocity field and assume that the temperature is given:

$$\boldsymbol{u} = \boldsymbol{0}, \qquad \theta = \theta_b. \tag{2.2}$$

Letting θ_s denote the saturation temperature (i.e. the temperature at which liquid and vapour phases are in thermodynamic equilibrium), we assume that the interfacial free-energy density ψ^{x} depends linearly on the interfacial temperature θ, so that†

$$\psi^{\mathrm{x}} = \psi_s^{\mathrm{x}} - \eta_s^{\mathrm{x}}(\theta - \theta_s), \tag{2.3}$$

where ψ_s^{x} and η_s^{x} are the constant values of the interfacial free-energy and entropy densities arising for $\theta = \theta_s$.‡ The interface conditions of Fried *et al.* (2006) then specialize to:

$$J = \rho(\boldsymbol{u}\cdot\boldsymbol{n} - V) = \rho^v(\boldsymbol{u}^v\cdot\boldsymbol{n} - V) = -\rho V^{mig}, \tag{2.4a}$$

$$\theta_s\eta_s^{\mathrm{x}}(KV - \nabla_s\cdot\boldsymbol{u}_s) = \kappa\nabla\theta\cdot\boldsymbol{n} - lV^{mig}, \tag{2.4b}$$

$$\frac{A}{6\pi h^3} + \boldsymbol{S}\boldsymbol{n}\cdot\boldsymbol{n} - \left(p - \frac{J^2}{\rho^v}\right) = \psi^{\mathrm{x}}K, \tag{2.4c}$$

$$\boldsymbol{S}\boldsymbol{n}\cdot\boldsymbol{t} = -\eta_s^{\mathrm{x}}\nabla_s\theta\cdot\boldsymbol{t}, \tag{2.4d}$$

$$\beta_s V^{mig} = -l\left(\frac{\theta}{\theta_s} - 1\right) - \left(p - \frac{J^2}{\rho^v}\right) + \tfrac{1}{2}\rho|\boldsymbol{u}|^2. \tag{2.4e}$$

Here, $\boldsymbol{n}$ and $\boldsymbol{t}$ denote the interfacial unit tangent and normal vectors, the latter being directed from the liquid into the vapour and K denotes the interfacial curvature. Also, $\boldsymbol{u}$ and $\boldsymbol{u}^v$ are the interfacial limits of the velocities in the liquid and vapour phases, $\boldsymbol{u}^i$ is the velocity describing the evolution of the liquid–vapour interface, $V = \boldsymbol{u}^i\cdot\boldsymbol{n}$ is the (scalar) normal velocity of the interface, $V^{mig} = V - \boldsymbol{u}\cdot\boldsymbol{n}$ is the velocity of the interface relative to the liquid velocity, and $\boldsymbol{u}_s = (\boldsymbol{u}\cdot\boldsymbol{t})\boldsymbol{t}$ is the tangential component of the velocity of the liquid at the liquid–vapour interface.

In (2.4*b–d*), ∇_s denotes the surface gradient. Given scalar and vector fields f and $\boldsymbol{f}$ defined on the surface, $\nabla_s f$ and $\nabla_s\cdot\boldsymbol{f}$ can be computed using the normally constant extensions f^e and $\boldsymbol{f}^e$ of f and $\boldsymbol{f}$ via $\nabla_s f = \mathbb{P}\nabla f^e$ and $\nabla_s\cdot\boldsymbol{f} = \mathbb{P} : \nabla\boldsymbol{f}^e$, where

$$\mathbb{P} = \mathbf{1} - \boldsymbol{n}\boldsymbol{n}$$

† Generally, there is a difference between the interfacial free-energy density ψ^{x} and the surface tension σ. When surfactant with interfacial molecular density n^{x} is taken into account, ψ^{x} and σ are related by $\psi^{\mathrm{x}} = \sigma + n^{\mathrm{x}}\mu - (\alpha + \lambda)\mathrm{tr}\,\mathbb{D}$, where μ is the chemical potential of the surfactant, $\mathbb{D} = \mathbb{P}\boldsymbol{D}\mathbb{P}$ is the interfacial stretching tensor, and $\lambda + \alpha > 0$ is the interfacial dilatational viscosity. When surfactant is absent, so that $n^{\mathrm{x}} = 0$ and the viscosities of the interface are of negligible importance, we have $\psi^{\mathrm{x}} = \sigma$. When surfactant is present, as is the case in § 5, we have $\psi^{\mathrm{x}} \neq \sigma$.

‡ Consistent with the notation of Fried *et al.* (2006), a superscript 'x' distinguishes an interfacial excess quantity (Gibbs 1878) from a bulk quantity.

denotes the interfacial projector (with $\boldsymbol{ab}$ being the dyadic product of two vectors $\boldsymbol{a}$ and $\boldsymbol{b}$, defined so that $(\boldsymbol{ab})\boldsymbol{c} = (\boldsymbol{b}\cdot\boldsymbol{c})\boldsymbol{a}$). In (2.4*c–d*), $\boldsymbol{S} = 2\rho\nu\boldsymbol{D}$ is the conventional Newtonian extra stress, where $\boldsymbol{D} = (\nabla\boldsymbol{u} + (\nabla\boldsymbol{u})^{\top})/2$ is the bulk rate-of-stretch. The parameters $l > 0$ and β_s are the latent heat of vaporization and a modulus associated with the kinetics of attachment and detachment at the interface. Further, A is the Hamaker constant – the value of which depends on the properties of the liquid and the substrate.

The system of interface conditions (2.4) involves two contributions in addition to those discussed by Burelbach *et al.* (1988). These include the term $\theta_s\eta_s^{\mathrm{x}}(KV - \nabla_s\cdot\boldsymbol{u}_s)$, in the energy balance (2.4*b*), which accounts for the transport of energy along the liquid–vapour interface. Physically, this term provides an additional mechanism for energy dissipation within the interface. To our knowledge, the influence of this term on liquid film evolution has not been studied previously in the literature. The other contribution is formed by the combination of the second and the third terms on the right-hand side of (2.4*e*), which can be viewed as an effective pressure accounting for vapour recoil through the combination $p - J^2/\rho^v$ and kinetic energy through $(1/2)\rho|\boldsymbol{u}|^2$. A condition similar to (2.4*e*) and relating the evaporation mass flux to the temperature difference and pressure was used by Moosman & Homsy (1980) to determine the shape of an evaporating liquid meniscus. The influence of this pressure term on the dynamics of an evaporating meniscus is also discussed by Wayner (1999). Note, however, that the presence of the vapour recoil term in the interfacial configurational momentum balance (2.4*e*) being distinct from that in the interfacial standard momentum balance (2.4*c*) has not been considered previously.

The goal of this paper is to investigate the influence of the energy flux along the interface and the effective pressure on the stability of the evaporating film. In the lubrication approximation used in this paper, the terms $\theta_s\eta_s^{\mathrm{x}}KV$ and $(1/2)\rho|\boldsymbol{u}|^2$ turn out to be small in comparison to the leading-order terms $-\theta_s\eta_s^{\mathrm{x}}\nabla_s\cdot\boldsymbol{u}_s$ and $p - J^2/\rho^v$; in the subsequent analysis, these leading-order terms are the dominant contributions to the interfacial energy flux and the effective pressure terms, correspondingly.

2.1. *Scaling of the model*

Letting h_0 denote a characteristic measure of the film thickness (e.g. the initial, undisturbed thickness of the film), we introduce the following dimensionless variables

$$\left.\begin{array}{ccccc} \tilde{\boldsymbol{x}} = \dfrac{\boldsymbol{x}}{h_0}, & \tilde{t} = \dfrac{\nu t}{h_0^2}, & \tilde{\boldsymbol{u}} = \dfrac{h_0\boldsymbol{u}}{\nu}, & \tilde{h} = \dfrac{h}{h_0}, & \tilde{p} = \dfrac{h_0^2 p}{\rho\nu^2}, \\ \tilde{J} = \dfrac{Lh_0 J}{\kappa\Delta\theta}, & \tilde{\theta} = \dfrac{\theta-\theta_s}{\Delta\theta}, & \tilde{\psi}^{\mathrm{x}} = \dfrac{\psi^{\mathrm{x}}}{\psi_s^{\mathrm{x}}}, & \tilde{\eta}^{\mathrm{x}} = \dfrac{\eta^{\mathrm{x}}}{\eta_s^{\mathrm{x}}}, & \end{array}\right\} \tag{2.5}$$

where

$$L = \frac{l}{\rho}$$

denotes the latent heat per unit mass and

$$\Delta\theta = \theta_b - \theta_s$$

denotes the temperature drop between the base and the free surface of the film. This scaling gives rise to the following dimensionless numbers:

$$\left.\begin{gathered} Pr = \frac{\rho c \nu}{\kappa}, \qquad M = \frac{h_0 \eta_s^{\mathrm{x}} c \Delta\theta}{2\kappa\nu}, \qquad D = \frac{\rho^v}{\rho}, \\ C = \frac{\eta_s^{\mathrm{x}} \Delta\theta}{\psi_s^{\mathrm{x}}}, \qquad \Sigma = \frac{h_0 \psi_s^{\mathrm{x}}}{\rho\nu^2}, \qquad \Pi = \frac{-A}{6\pi h_0 \rho \nu^2}, \qquad E = \frac{\kappa\Delta\theta}{\rho\nu L}, \\ N = \frac{\eta_s^{\mathrm{x}} \nu \theta_s}{h_0 \kappa \Delta\theta}, \qquad A_1 = \frac{\beta_s \kappa \theta_s}{\rho l h_0 L}, \qquad A_2 = \frac{\rho \nu^2 \theta_s}{h_0^2 l \Delta\theta}. \end{gathered}\right\} \tag{2.6}$$

Here, Pr and M are Prandtl and Marangoni numbers; D is the ratio of the density of the vapour phase to that of the liquid phase; C and Σ are the capillary and the reverse capillary numbers; Π is the dimensionless Hamaker constant; E is the evaporation number; N is a parameter which accounts for the energy flux along the interface; A_1 characterizes how far the system is from thermodynamic equilibrium; A_2 accounts for the magnitude of the effective pressure.

Dropping the superposed tildes from the dimensionless variables (2.5), the scaled bulk evolution equations following from (2.1) are:

$$\begin{gathered} \frac{\mathrm{D}\boldsymbol{u}}{\mathrm{D}t} = -\nabla p + \nabla^2 \boldsymbol{u} \\ Pr \frac{\mathrm{D}\theta}{\mathrm{D}t} = \nabla^2 \theta, \\ \nabla \cdot \boldsymbol{u} = 0; \end{gathered}$$

the dimensionless boundary conditions on the substrate following from (2.2) are:

$$\boldsymbol{u} = \boldsymbol{0}, \qquad \theta = 1; \tag{2.7a, b}$$

the conditions at the liquid–vapour interface following from (2.4) are:

$$EJ = \boldsymbol{u}\cdot\boldsymbol{n} - V, \tag{2.8a}$$

$$N(KV - \nabla_s \cdot \boldsymbol{u}_s) = \nabla\theta \cdot \boldsymbol{n} + J, \tag{2.8b}$$

$$\frac{\Pi}{h^3} - p + 2\boldsymbol{D}\boldsymbol{n}\cdot\boldsymbol{n} = -\frac{E^2 J^2}{D} + \Sigma K(1 - C\theta), \tag{2.8c}$$

$$-\boldsymbol{D}\boldsymbol{n}\cdot\boldsymbol{t} = \frac{M}{Pr}\nabla_s\theta\cdot\boldsymbol{t}, \tag{2.8d}$$

$$A_1 J = \theta + A_2\left(p - E^2 D^{-1} J^2 - \tfrac{1}{2}\boldsymbol{u}^2\right).$$

Assuming that the horizontal scale of the liquid motion is significantly larger than the vertical one and that the time evolution is slow enough, a long-wave approximation can be applied. Writing X, Z, U and W for the long-wave dimensionless counterparts of x, z, u and w; P, Θ and H for the variables corresponding to dimensionless pressure, temperature, and the film thickness, we derive the leading-order equations following the procedure described by Williams & Davis (1982). Details of the derivation are given in the Appendix. The leading-order dimensionless problem consists of: bulk equations

$$-P_X + U_{ZZ} = 0, \tag{2.9a}$$

$$-P_Z = 0, \tag{2.9b}$$

$$\theta_{ZZ} = 0, \tag{2.9c}$$

$$U_X + W_Z = 0; \tag{2.9d}$$

boundary conditions at the solid substrate

$$W = 0, \qquad U = 0, \qquad \Theta = 1; \tag{2.10}$$

and boundary conditions at the liquid–vapour interface $Z = H(X, T)$

$$\bar{E} J = -H_T - H_X U + W, \tag{2.11a}$$

$$\bar{N} \mathscr{V}_X = -\Theta_Z - J, \tag{2.11b}$$

$$P = \bar{E}^2 \bar{D}^{-1} J^2 + \frac{\bar{\Pi}}{H^3} - \bar{\Sigma} H_{XX}, \tag{2.11c}$$

$$\tfrac{1}{2} U_Z + \frac{\bar{M}}{Pr}(\Theta_X + H_X \Theta_Z) = 0, \tag{2.11d}$$

$$A_1 J = \Theta + \bar{A}_2 (P - \bar{E}^2 \bar{D}^{-1} J^2). \tag{2.11e}$$

Equations (2.9*b*) and (2.9*c*) indicate that, to leading order, the dimensionless pressure P is independent of the vertical coordinate Z and the dimensionless temperature Θ is a linear function of Z. Applying the boundary condition (2.11*c*) at $Z = H$, we obtain

$$P = \bar{E}^2 \bar{D}^{-1} J^2 + \frac{\bar{\Pi}}{h^3} - \bar{\Sigma} h_{XX},$$
$$\Theta = 1 + c_1 Z,$$

where c_1 depends on X and T. Integration of (2.9*a*, *d*) gives explicit representations

$$U(Z) = \frac{P_X}{2} Z(Z - H) + \frac{\mathscr{V}}{H} Z$$

and

$$W(Z) = -\frac{P_{XX}}{2}\left(\frac{Z^3}{3} - \frac{HZ^2}{2}\right) + \frac{P_X}{4} Z^2 H_X - \left(\frac{\mathscr{V} Z^2}{2H}\right)_X$$

for the velocity components U and W in terms of the unknown height H and unknown horizontal component $\mathscr{V}$ of the liquid velocity at the interface. Expressing the pressure P in (2.11*e*) through (2.11*c*) we obtain

$$A_1 J = \Theta - \bar{A}_2 \left(\bar{\Sigma} H_{XX} - \frac{\bar{\Pi}}{H^3}\right),$$

which determines the constant c_1 as

$$c_1(J) = \left[A_1 J - 1 + \bar{A}_2 \left(\bar{\Sigma} H_{XX} - \frac{\bar{\Pi}}{H^3}\right)\right] \frac{1}{H}.$$

To simplify notation, we return to the original variables. To the leading-order, the solution to the problem (2.9)–(2.11) splits into two subsystems. The first subsystem, which determines how u, w and θ depend on z, has the form

$$u(z) = \frac{p_x}{2} z(z - h) + \frac{\mathscr{V}}{h} z, \tag{2.12a}$$

$$w(z) = -\frac{p_{xx}}{2}\left(\frac{z^3}{3} - \frac{hz^2}{2}\right) + \frac{p_x}{4} z^2 h_x - \left(\frac{\mathscr{V} z^2}{2h}\right)_x, \tag{2.12b}$$

$$\theta(z) = 1 + \left[A_1 J - 1 + A_2 \left(\Sigma h_{xx} - \frac{\Pi}{h^3}\right)\right] \frac{z}{h}. \tag{2.12c}$$

From (2.12), knowledge of p, h, $\mathscr{V}$ and J is sufficient to determine u, w and θ. The second subsystem determines the long-wave evolution of the system and has the form

$$p = E^2 D^{-1} J^2 + \frac{\Pi}{h^3} - \Sigma h_{xx} \tag{2.13a}$$

$$EJ = -h_t + \tfrac{1}{12}(p_x h^3)_x - \tfrac{1}{2}(\mathscr{V} h)_x, \tag{2.13b}$$

$$N\mathscr{V}_x = \left[1 - A_1 J - A_2\left(\Sigma h_{xx} - \frac{\Pi}{h^3}\right)\right]\frac{1}{h} - J, \tag{2.13c}$$

$$\frac{p_x h}{2} + \frac{\mathscr{V}}{h} + 2MP^{-1}\left[A_1 J_x + A_2\left(\Sigma h_{xxx} + \frac{3h_x \Pi}{h^4}\right)\right] = 0. \tag{2.13d}$$

This set of equations represents a closed system for the unknown variables p, h, $\mathscr{V}$ and J. In the system (2.13), the term with coefficient A_2 introduces capillary and disjoining pressure effects into the energy and momentum balance equations (2.13c) and (2.13d). It is important to note that in the momentum balance, the dimensionless numbers MA_1/P and $MA_2\Sigma/P$ accounting for mass flux and capillary pressure are both independent of the scale h_0 of the film thickness.

When there is no entropy transport along the film surface and the effective pressure is neglected, so that $N = A_2 = 0$, the system (2.13) can be reduced to a single evolution equation of the form

$$h_t + \frac{E}{A_1 + h} + \left[\left(\frac{2E^2 h^3}{3D(A_1+h)^3} + \frac{\Pi}{h} + \frac{MA_1 h^2}{P(A_1+h)^2}\right)h_x + \frac{\Sigma h^3 h_{xxx}}{3}\right]_x = 0.$$

This equation was studied in detail by Burelbach *et al.* (1988). For this reason, in the following analysis we focus our attention on influences of the entropy transport ($N \neq 0$) and the effective pressure ($A_2 \neq 0$) terms on the film evolution and stability.

3. Base state

The base state of the evaporating film is time dependent. Assuming that changes in film thickness occur only because of evaporation and that otherwise the film is motionless ($\boldsymbol{u} = \boldsymbol{0}$) with properties independent of the x-coordinate (so that all derivatives with respect to x vanish), we rewrite the governing equations (2.7a, b) in the form:

$$\hat{p}_z = 0, \tag{3.1a}$$

$$Pr\,\hat{\theta}_t = \hat{\theta}_{zz}. \tag{3.1b}$$

Since $\boldsymbol{u} = \boldsymbol{0}$, the incompressibility equation $\nabla \cdot \boldsymbol{u} = 0$ is trivially satisfied. Here a superposed hat is used to denote a variable describing the time-dependent base state. The boundary condition (2.7b) on the substrate reduces to

$$\hat{\theta} = 1; \tag{3.2}$$

at the liquid–vapour interface, the boundary conditions (2.8) become

$$E\hat{J} = -\hat{h}_t, \tag{3.3a}$$

$$\hat{J} = -\hat{\theta}_z, \tag{3.3b}$$

$$\hat{p} = E^2 D^{-1}\hat{J}^2 + \frac{\Pi}{\hat{h}^3}, \tag{3.3c}$$

$$A_1\hat{J} = \hat{\theta} + \frac{A_2\Pi}{\hat{h}^3}. \tag{3.3d}$$

Equation (3.1*b*) has exponentially decaying time-dependent solutions. To solve the stability problem, we will use perturbations in the form of normal modes which may grow exponentially in time. We therefore consider such a quasi-static limit of the base state problem (3.1)–(3.3), for which the slow evolution of the base state may be neglected relative to exponentially growing perturbations developing on top of the base state. This can be achieved in the following two cases.

(i) Case $E \ll 1$ of slow evaporation but Prandl number Pr of $O(1)$. It is then convenient to make the transformation $(z, t) \mapsto (z, Et)$ and seek a solution in powers of E:

$$\begin{aligned}\hat{p} &= E^{-1}(p_0 + Ep_1 + \cdots),\\ \hat{\theta} &= \theta_0 + E\theta_1 + \cdots,\\ \hat{J} &= J_0 + EJ_1 + \cdots.\end{aligned}$$

Assuming that D, Π and A_2 can be represented as $D = E^3\bar{D}$, $\Pi = E\bar{\Pi}$ and $A_2 = \bar{A}_2/E$, where $\bar{D} \sim \bar{\Pi} \sim \bar{A}_2 \sim O(1)$, the resulting leading-order system is:

$$\begin{aligned} & p_{0_z} = 0,\\ & \theta_{0_{zz}} = 0,\\ z = 0: \quad & \theta_0 = 1,\\ z = \hat{h}(t): \quad & \begin{cases} J_0 = -\hat{h}_t,\\ J_0 = -\theta_{0_z},\\ p_0 = E^3 D^{-1} J_0^2 + \dfrac{E\Pi}{\hat{h}^3},\\ A_1 J_0 = \theta_0 + \dfrac{A_2\Pi}{\hat{h}^3}. \end{cases}\end{aligned} \tag{3.4}$$

(ii) Case $Pr \ll 1$ of small Prantdl number but evaporation number E of $O(1)$. This case is relevant to molten metals, for which the Prandtl number is of the order of 10^{-3} to 10^{-2}. Under these circumstances, a solution can be sought in powers of Pr:

$$\begin{aligned}\hat{p} &= Pr^{-1}(p_0 + Pr\, p_1 + \cdots),\\ \hat{\theta} &= \theta_0 + Pr\,\theta_1 + \cdots,\\ \hat{J} &= J_0 + Pr\, J_1 + \cdots.\end{aligned}$$

Assuming that $D = Pr\,\bar{D}$, $\Pi = Pr\,\bar{\Pi}$ and $A_2 = \bar{A}_2/Pr$, where $\bar{D} \sim \bar{\Pi} \sim \bar{A}_2 \sim O(1)$, we arrive at:

$$\begin{aligned} & p_{0_z} = 0,\\ & \theta_{0_{zz}} = 0,\\ z = 0: \quad & \theta_0 = 1,\\ z = \hat{h}(t): \quad & \begin{cases} EJ_0 = -\hat{h}_t,\\ J_0 = -\theta_{0_z},\\ p_0 = Pr\, E^2 D^{-1} J_0^2 + \dfrac{Pr\,\Pi}{\hat{h}^3},\\ A_1 J_0 = \theta_0 + \dfrac{A_2\Pi}{\hat{h}^3}. \end{cases}\end{aligned} \tag{3.5}$$

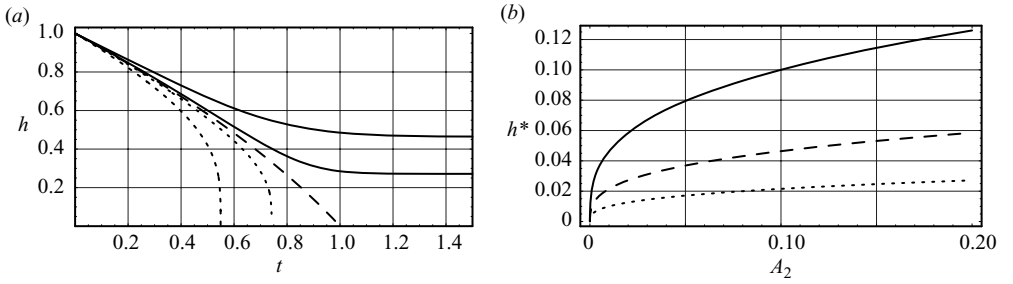

FIGURE 2. (*a*) Evolution of the film thickness for different parameters A_2. $A_2 = 20$, $A_2 = 100$ (dotted lines); $A_2 = -20$, $A_2 = -100$ (solid lines). Time is measured in the units of disappearance time for the case $A_2 = 0$ (dashed line). (*b*) Film thickness as the function of the parameter A_2: $h^* = (-A_2\Pi)^{1/3}$ for $\Pi = 1 \times 10^{-4}$ (dotted line), $\Pi = 1 \times 10^{-3}$ (dashed line), $\Pi = 1 \times 10^{-2}$ (solid line).

To the leading order, the solution to the systems (3.4) and (3.5) can be represented in the original variables as:

$$\hat{h}_t = -\frac{1 + A_2\Pi/\hat{h}(t)^3}{A_1 + \hat{h}(t)}E, \tag{3.6a}$$

$$\hat{J}(t) = -\hat{h}_t/E, \tag{3.6b}$$

$$\hat{\theta}(t) = 1 - \hat{J}(t)z, \tag{3.6c}$$

$$\hat{p}(t) = E^2 D^{-1}\hat{J}(t)^2 + \frac{\Pi}{\hat{h}(t)^3}. \tag{3.6d}$$

The nonlinear ordinary differential equation (3.6*a*) was integrated numerically using the Runge–Kutta method. Typical values of the Hamaker constant are usually small. According to Wayner (1998), the Hamaker constants for water, ethanol and benzine are 3.7×10^{-20} J, 3.6×10^{-20} J and 5×10^{-20} J, respectively. If we neglect the dimensionless parameter $A_2\Pi$, which is small (for water, $A_2\Pi \sim 10^{-5}$) in comparison to 1 in the numerator of (3.6), the base state takes the simple form $\hat{h}(t) = -A_1 + \sqrt{(A_1+1)^2 - 2Et}$ investigated by Burelbach *et al.* (1988). Note that the solution to (3.6) does not satisfy the arbitrary initial temperature distribution across the layer and has a singularity at the disappearance time t_d when $A_1 = 0$ and $h = 0$. Burelbach *et al.* (1988) addressed these issues and showed that nevertheless the solution provides a good approximation in the intermediate time regime. Also we can see that the energy flux characterized by N does not affect the base state (3.6).

Equation (3.6) suggests that, for small enough film thickness h, the base state is influenced by the disjoining pressure term proportional to A_2. Depending on the properties of the liquid and the underlying substrate, we can expect cases where the film partially ($\Pi > 0$) or completely ($\Pi < 0$) wets the substrate. For $\Pi > 0$, the film ruptures once it thins to a certain critical thickness. The evolution of the film thickness in the base state according to (3.6) is presented in figure 2(*a*) with dotted lines. All parameters except A_2 are for water. In this case, increasing A_2 reduces t_d. Note that the effect is small. To demonstrate it, we took $A_2 = 100$. For water, A_2 is ~ 0.01. Our choice is therefore unrealistically large and is made only to suggest what may happen for other substances. The solution shown with the dashed line indicates the demarking case $A_2 = 0$.

Burelbach *et al.* (1988) ($A_2 = 0$ in (3.6*a*)) showed that the vertical velocity h_t behaves as $h_t \sim 1/(A_1 + h)$ when $h \to 0$. Therefore in the limiting case of $A_1 = 0$, the lubrication approximation breaks down. In contrast to this, the evolution equation (3.6*a*) shows that, in the presence of non-vanishing effective pressure, the expression for h_t is always singular, even for the cases when $A_1 \neq 0$, and that changes in the base state occur even faster. Specifically, $h_t \sim A_2/(A_1 + h)h^3$ as $h \to 0$. The reduction of the disappearance time owing to the disjoining pressure imposes even stricter limitations on the range in which the lubrication approximation is valid. Also, this result demonstrates the importance of the effective pressure term in problems of the nonlinear film evolution leading to rupture.

For the case $\Pi < 0$, van der Waals forces are able to prevent further evaporation when the film reaches the critical thickness (as determined by the case $\Pi > 0$) and the liquid film forms a thin layer that covers the substrate without rupturing. A discussion of the situation when the van der Waals forces suppress evaporation from the adsorbed liquid film in systems where the liquid completely wets the substrate is given by Moosman & Homsy (1980) and by Wayner (1999) for a meniscus. The evolution of the film thickness base state for the case $\Pi < 0$ is shown with solid lines in figure 2(*a*). At the moment t^* when the disjoining pressure suppresses evaporation, a new stationary-state solution ('adsorbed layer') is achieved. We determine such a solution by setting h_t in (3.6*a*) equal to zero. This solution is characterized by zero mass flux, constant temperature across the layer, and pressure given by the disjoining pressure:

$$h^* = (-A_2\Pi)^{1/3}, \tag{3.7a}$$

$$J^* = 0, \tag{3.7b}$$

$$\theta^* = 1, \tag{3.7c}$$

$$p^* = \frac{\Pi}{(h^*)^3} = \frac{1}{-A_2}. \tag{3.7d}$$

Depending on the parameters characterizing the liquid and the substrate, the thickness of this stationary layer varies according to (3.7). The dependence of the dimensionless layer thickness h^* on the parameter A_2 is shown in figure 2(*b*) for different values of the dimensionless Hamaker constant Π. Even though the relative magnitudes of the coefficients A_2 and Π are small, the figure shows that we can expect to obtain a film thickness of one or a few monolayers. To see explicitly which physical variables affect the thickness h of the layer (3.7*a*), we use dimensional quantities to give:

$$h = \left(\frac{-A\,\theta_s}{6\pi h_0^3 l\,\Delta\theta}\right)^{1/3}.$$

This expression agrees with the estimate for the adsorbed film thickness obtained by Wayner (1999). We see that for $A < 0$, the thickness h increases with the saturation temperature θ_s and the magnitude $|A|$ of the dimensional Hamaker constant. Also h decreases with the latent heat of vaporization and with increasing values of the initial temperature difference $\Delta\theta$ across the layer.

The results of this section (table 1) show that, since the base state is independent of the horizontal coordinate, the structure is not affected by the energy flux along the liquid–vapour interface. The influence of the effective pressure increases toward the disappearance time. In the absence of the effective pressure, the base state is insensitive to the sign of the Hamaker constant and, therefore, there is a degeneracy with respect

Variable	Units	Water	Sodium
θ_s	K	373	1156
$\Delta\theta$	K	10	2
ρ	$\mathrm{kg\,m^{-3}}$	960	750
ν	$\mathrm{m^2\,s^{-1}}$	3×10^{-7}	2×10^{-7}
κ	$\mathrm{J\,m^{-1}\,s^{-1}\,K^{-1}}$	0.68	48
c	$\mathrm{J\,kg^{-1}\,K^{-1}}$	4166	1280
L	$\mathrm{J\,kg^{-1}}$	2.3×10^6	4.24×10^6
η_s^{x}	$\mathrm{N\,m^{-1}\,K^{-1}}$	1.8×10^{-4}	0.94×10^{-4}
ψ_s^{x}	$\mathrm{N\,m^{-1}}$	5.89×10^{-2}	1.2×10^{-1}
A	J	10^{-20}	10^{-21}
β_s	$\mathrm{kg\,m^{-2}\,s^{-1}}$	10^6	10^6

TABLE 1. Material properties of water and molten sodium. Parameters are taken near the boiling temperature.

to the cases when liquid partially or absolutely wets the substrate. The presence of the effective pressure alleviates this degeneracy and leads to a rich spectrum of solutions that evolve from the base state.

4. Linear stability of the film

To investigate the stability of the system (2.13) we perturb the time-dependent base state in the form

$$h(t, x) = \hat{h}(t) + H(t)\mathrm{e}^{\mathrm{i}kx}, \tag{4.1a}$$

$$J(t, x) = \hat{J}(t) + J(t)\mathrm{e}^{\mathrm{i}kx}, \tag{4.1b}$$

$$V(t, x) = \mathrm{i}V(t)\mathrm{e}^{\mathrm{i}kx}, \tag{4.1c}$$

where k is the wavenumber, and obtain an ordinary differential equation

$$\dot{H}/H = F(t, k, A_1, A_2, D, E, M, Pr, N, \Pi, \Sigma) \tag{4.2}$$

describing the evolution of disturbances to the interface. Integrating (4.2) over t from $t = 0$ to $t = t^*$, with $t^* < t_d$, we have

$$H(t^*) = H(0)\exp(\sigma(t^*)t^*),$$

where

$$\sigma(t^*) = \frac{1}{t^*}\int_0^{t^*} F(t, k, A_1, A_2, D, E, M, Pr, N, \Pi, \Sigma)\,\mathrm{d}t$$

is an effective growth rate which is calculated numerically. We also assume that there exists a limiting case of a time-independent base state, frozen at the instant $t = 0$. For this case, in (4.1) we take $\hat{h} = 1$ and $\hat{J} = (1 + A_2\Pi)/(A_1 + 1)$ and we use the following expression for the growth rate:

$$\omega = F(0, k, A_1, A_2, D, E, M, Pr, N, \Pi, \Sigma). \tag{4.3}$$

Numerical experiments performed with different parameter values showed that the evaporation number E exerts a significant influence on stability. To demonstrate this influence, we plot in figure 3 the effective growth rate ω for increasing values of E,

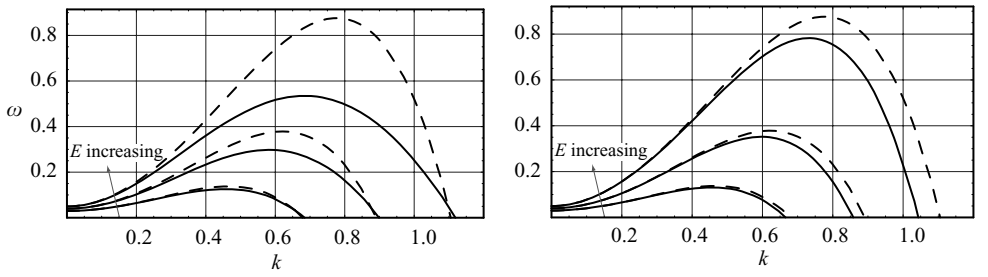

FIGURE 3. Three pairs of dispersion curves for increasing values of the evaporation number $E = 0.03$, $E = 0.04$ and $E = 0.05$. (a) Change due to the influence of N. Dashed curve indicate cases with $N = A_2 = 0$. Solid curves show cases with $N = 0.3$ and $A_2 = 0$. (b) Change due to the influence of A_2. Dashed curve shows the case $N = A_2 = 0$. Solid curves show the case $N = 0$ and $A_2 = 0.015$.

Parameter	Water	Sodium
A_1	5.2×10^{-3}	0.55
A_2	1.5×10^{-2}	0.054
D	6.25×10^{-4}	3.0×10^{-4}
E	0.010	0.15
M	0.18	1.2×10^{-4}
N	0.30	0.022
Pr	1.76	0.004
Σ	6.81	40
Π	6.1×10^{-4}	1.8×10^{-4}

TABLE 2. Dimensionless parameters at $h_0 = 100\,\text{Å}$.

taking all other dimensionless parameters for water (table 2). The parameter sequence $E = 0.03$, $E = 0.04$, $E = 0.05$ corresponds to three pairs of dispersion curves with increasing maximal growth rate ω. Each pair consists of a solid and a dashed curve. Figure 3(a) shows the influence of the evaporation number on the energy transport on the surface as determined by the dimensionless number N. This influence is given by the difference between the solid and dashed curves in each pair. The dashed curves indicate cases with $N = A_2 = 0$; the solid curves show cases with $N = 0.3$ and $A_2 = 0$. In the same way, figure 3(b) exhibits the influence of the evaporation number E on the effective pressure. The dashed curves indicate cases with $N = A_2 = 0$; the solid curves show the cases with $N = 0$ and $A_2 = 0.015$.

The results presented in figure 3 indicate that the effects of the energy transport along the surface as well as the effective pressure on the stability of the liquid film (as given by the difference between the solid and the dashed curves in each pair) both increase with increasing evaporation number E. The values of E used to demonstrate this effect are somewhat larger than the actual value $E = 0.01$ of the evaporation number for water. According to our discussion of the base state in § 3, large evaporation numbers make it impossible to use the slow evaporation limit, which is relevant for regular fluids when the evaporation number obeys $E \ll 1$ and the Prandtl number is $O(1)$. To proceed with our analysis we therefore use the alternative type of base state valid for circumstances where the Prandtl number obeys $Pr \ll 1$

Material	$E = \kappa \Delta\theta / \rho \nu L$
Water	0.001
Ethanol	0.0005
Mercury	0.189
Lead	0.022
Potassium	0.098
Sodium	0.075

TABLE 3. Evaporation number for some materials at ($\Delta\theta = 1$ K).

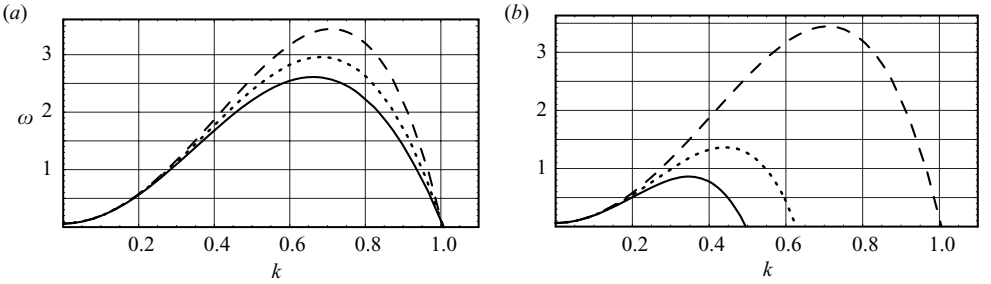

FIGURE 4. The influence of the interfacial energy flux and the effective pressure on the dispersion curve. (*a*) $A_2 = 0$ for all curves. $N = 0$ (dashed curve), $N = 0.011$ (dotted curve), $N = 0.022$ (solid curve). (*b*) $N = 0$ for all curves. $A_2 = 0$ (dashed curve), $A_2 = 0.025$ (dotted curve), $A_2 = 0.05$ (solid curve).

and the evaporation number is $O(1)$. Molten metals seem to be good candidates for this purpose. As the data in tables 2 and 3 show, they have small Prandtl numbers and relatively large evaporation numbers E.

As a representative example of a molten metal, we consider molten sodium. A detailed description of the properties of sodium is given by Foust (1972). The configurational momentum balance contains the modulus β_s associated with the kinetics of attachment and detachment at the interface. This modulus enters the dimensionless parameter A_1. To make reasonable estimates of the magnitude of β_s, we used experimental data relating the evaporating mass flux J with the pressure deviation $p - p_v$, where p_v is the pressure of the vapour phase. Substituting these data into the truncated version

$$\beta_s = \frac{\rho}{J}\left(p - \frac{J^2}{\rho_v}\right)$$

of the configurational momentum balance (2.4*c*), we obtained rough estimates for β_s. Experimental data obtained by Yang *et al.* (1994) and Fedkin, Grossman & Ghiorso (2005) then give β_s values of the order of 10^6 and $10^5\,\mathrm{kg\,m^{-2}\,s^{-1}}$, respectively. These values agree with estimates for coefficient A_1 used by Ajaev & Homsy (2001).

The influences of dimensionless parameters on the dispersion curves are presented in figure 4 for molten sodium (table 2). Figure 4(*a*) demonstrates the influence of the surface energy flux as characterized by the dimensionless parameter N. The solid line represents the behaviour of the growth rate ω for the parameter $N = N_{\mathrm{Na}}$ for molten sodium. The dashed line shows the case $N = 0$ of no energy flux along the liquid–vapour interface. The dotted line shows the case $N = N_{\mathrm{Na}}/2$. The dynamics of

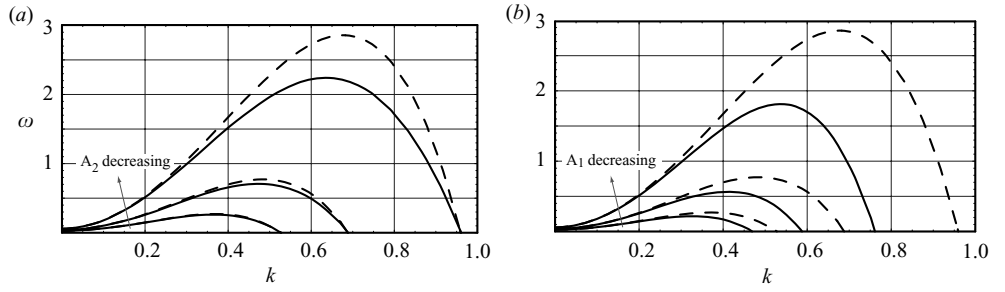

FIGURE 5. Three pairs of the dispersion curves for increasing parameter $A_1 = 0.6$, $A_1 = 1$, $A_1 = 1.4$. (*a*) Change in the influence of N. Dashed curves indicate cases with $N = A_2 = 0$, solid curves show cases with $N = 0.022$, $A_2 = 0$. (*b*) Change in the influence of A_2. Dashed curve shows the case $N = A_2 = 0$. Solid curves shows the case $N = 0$, $A_2 = 0.01$.

these changes demonstrate that the increase of the energy flux on the film surface decreases the maximal growth rate. The corresponding wavenumber slowly decreases while the cutoff wavenumber slowly increases and thereby broadens the interval of unstable modes.

Figure 4(*b*) demonstrates the influence of the effective pressure as characterized by the dimensionless parameter A_2. The solid line represents the behaviour with the parameter $A_2 = (A_2)_{\mathrm{Na}}$ for molten sodium. The dashed line shows the case $A_2 = 0$ for which the effective pressure is absent. The dotted line shows the case $A_2 = (A_2)_{\mathrm{Na}}/2$. Increasing A_2 narrows the interval of the unstable modes and decreases the maximal growth rate. We therefore observe that the effective pressure exerts a stabilizing influence on a film of molten sodium.

The stabilizing influences of the interfacial energy flux and the effective pressure seem reasonable if we recall that both effects arise from dissipative mechanisms (Fried *et al.* 2006). Another quantity strongly affecting the stability results is the parameter A_1, describing how far the system is from the saturation equilibrium. To examine the changes this parameter causes, we use dimensionless parameters for molten sodium and plot the growth rate ω for three different values of A_1 (figure 5). The increasing parameter sequence $A_1 = 0.6$, $A_1 = 1$, $A_1 = 1.4$, corresponds to three pairs of curves with decaying maximal growth rate ω. The dashed curves represent the cases with $N = A_2 = 0$. The solid curves show the case with $N = 0.022$ and $A_2 = 0$ (figure 5*a*) and the case with $N = 0$ and $A_2 = 0.01$ (figure 5*b*). We see that A_1 exerts a strong stabilizing influence on the system. With A_1 increasing, the maximal effective growth rate decays and the cutoff wavenumber decreases. The relative influence (difference between the solid and dashed curves in the corresponding pictures) of the interfacial energy flux (figure 5*a*) and the effective pressure (figure 5*b*) decreases as the parameter A_1 increases. This result implies that the surface energy flux and the effective pressure both exert considerable influence on the stability of a molten metal film only when the film is far enough from saturation equilibrium.

To examine how the characteristic thickness h_0 of the film influences the stability of the system, we fix all parameters characterizing the physical properties of the system independent of h_0 and study the impact of varying h_0. In so doing, we consistently recalculate all dimensionless parameters depending on h_0. The behaviour of the dimensional maximal growth rate w_m (in units of s^{-1}, where w_m is maximized over the range of unstable wavenumbers) is shown in figure 6(*a*) for three particular

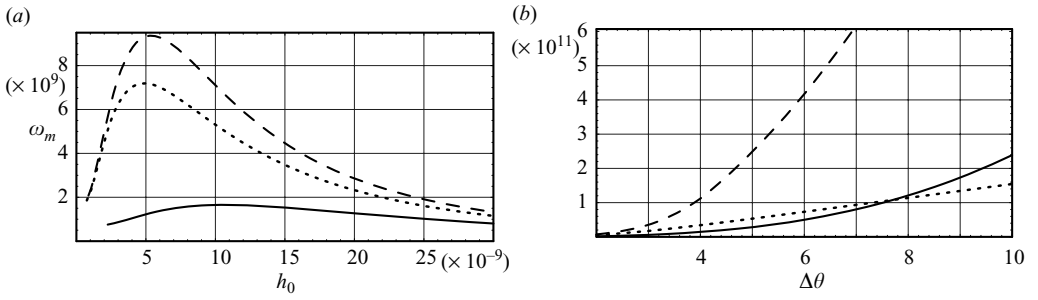

FIGURE 6. Change in the dimensional maximal growth rate ω_m (in units of s^{-1}) due to the change of (a) the initial dimensional layer thickness h_0 (in units of m) at fixed temperature difference $\Delta\theta = 2K$, (b) the dimensional temperature difference $\Delta\theta$ (K) at fixed layer thickness $h = 100$ Å. The dashed curve shows the case with $N = 0 = A_2 = 0$; the dotted line shows the case with $N = 0.022$, $A_2 = 0$; the solid curve shows the case with $N = 0$, $A_2 = 0.05$.

cases. The dashed line indicates the dependence with no interfacial energy flux and no effective pressure ($N = A_2 = 0$). The dotted line shows the case $A_2 = 0$ and $N = 0.022$, for which only the influence of the interfacial energy flux is taken into account. The solid line demonstrates the case $A_2 = 0.015$ and $N = 0$, for which only the effective pressure is taken into account. We see that the stabilizing influence of the effective pressure (difference between the solid and the dashed lines) is stronger than that of the interfacial energy flux (difference between the solid and the dotted lines). Moreover, the maximal growth rate ω_m is not a monotonic function of h_0. In the case of the presence of the effective pressure only (the solid curve), the largest value of ω_m corresponds to larger initial film thicknesses h_0 relative to the case $A_2 = 0$, $N = 0.022$ (the dashed curve). On its own, the interfacial energy flux (the dotted curve) moves the maximal growth rate ω_m to the thinner initial film thicknesses h_0. The figure also shows that both effects are important for the stability of molten metal films with thickness of 5–30 nm. Films of such thicknesses are common in applications such as welding (Winkler & Amberg 2005).

Similarly in figure 6(b), we consider the change in stability that results when the dimensional temperature difference $\Delta\theta$ across the film changes from 0 to 10 K. We fix parameters that characterize the physical properties of the system independent of $\Delta\theta$ and study the impact of varying $\Delta\theta$ while recalculating all dimensionless parameters depending on $\Delta\theta$. For this purpose, the initial film thickness remains fixed at $h_0 = 100$ Å. The dashed lines represents the case of zero interfacial energy flux ($N = 0$) and zero effective pressure ($A_2 = 0$). The dotted line shows the case with $A_2 = 0$ and $N = 0.022$. The solid line represents the case $A_2 = 0.015$ and $N = 0$. Again, we see the strong stabilizing influence of both effects relative to the case $N = A_2 = 0$. As the temperature difference across the layer increases, the influences of the effective pressure and the energy flux become more important.

From the base state time behaviour (figure 2), we expect the influence of all considered effects to increase as the instant t_d of disappearance is approached. The effective growth rate $\sigma(t^*)$ as a function of the wavenumber is shown in figure 7 at three different instants of time. We see that, in contrast to the results presented by Burelbach *et al.* (1988), the maximal growth rate is not a monotonic function of time for chosen parameter values. As t tends to t_d, the cutoff wavenumber increases – i.e. the interval of the unstable modes becomes wider and the system becomes more unstable. Figure 7 demonstrates that, for the chosen parameters, the stability of the

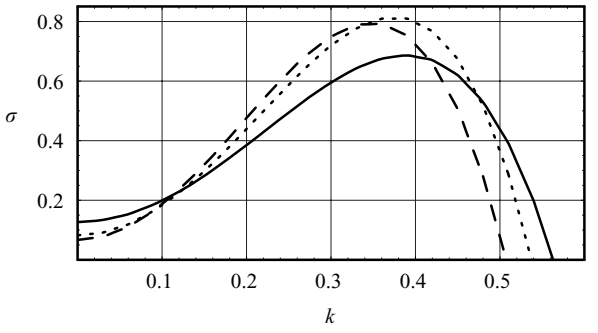

FIGURE 7. Effective growth rate at different times: $t = t_d/10$ (dashed line), $t = t_d/2$ (dotted line), $t = 9t_d/10$ (solid line), where $t_d = (2A_1 + 1)/2E$ and $A_2 = 0.05$, $N = 0.022$.

base state (3.6) does not change significantly for $t < t_d$. The effect is made evident on comparing the results for σ ($t \neq 0$) shown in figure 7 to the results for ω ($t = 0$) shown with the solid curve ($A_2 = 0.05$) in figure 4(*b*). Therefore the influences of the effective pressure and the energy flux along the surface remain important for all stages of the base-state evolution. The stability results for σ quantitatively alter the corresponding results for ω presented in figures 3–6 without inducing a qualitative change of the reported effects.

The results of this section reveal that, for the parameter values considered, the interfacial energy flux, governed by N, and the effective pressure, governed by A_2, stabilize the liquid layer. The film stability is more sensitive to variations of the effective pressure than to the interfacial energy flux. In particular, the effective pressure term strongly affects the cutoff wavenumber. The strong stabilizing effect of the effective pressure may be explained by the presence of the additional (relative to the case $A_2 = 0$) capillary terms in the energy balance (2.13*c*) and in the tangential momentum ballance (2.13*d*). Capillarity suppresses short waves and shifts the cutoff wavenumber in the direction of long waves figure 4(*b*). Also, we see that the parameter A_1, characterizing the closeness of the system to the saturation equilibrium, exerts a substantial influence.

5. Stability of the film with surfactant

In this section, we consider the influence of the interfacial energy flux and the effective pressure on the stability of a liquid film consisting of a volatile solvent and a non-volatile surfactant. A stability analysis for water-like liquids and common surfactants is given by Danov *et al.* (1998). Based on the foregoing results, we focus here on molten metals. For such liquids, dopants such as oxygen and sulfur play roles analogous to surfactants in conventional liquids and, as such, are commonly referred to as surfactants (Winkler & Amberg 2005). In this case, the expression (2.3) for the interfacial energy ψ^{x} is replaced by

$$\psi^{\mathrm{x}} = \psi_s^{\mathrm{x}} - \mu_s n^{\mathrm{x}} - \eta_s^{\mathrm{x}}(\theta - \theta_s),$$

where the chemical potential μ is defined as $\mu = \partial\psi^{\mathrm{x}}/\partial n$ and μ_s is its constant value at $\theta = \theta_s$.

The presence of the surfactant introduces additional terms into the system of interface conditions (Fried *et al.* 2006), so that (2.4*a*)–(2.4*e*) are modified to become:

$$J = \rho(\boldsymbol{u}\cdot\boldsymbol{n} - V) = \rho^{v}(\boldsymbol{u}^{v}\cdot\boldsymbol{n} - V), \tag{5.1a}$$

$$\theta_s \eta_s^{\mathrm{x}}(KV - \nabla_s\cdot\boldsymbol{u}_s) = \kappa\nabla\theta\cdot\boldsymbol{n} - lV^{mig}, \tag{5.1b}$$

$$\frac{A}{6\pi h^3} + \boldsymbol{S}\boldsymbol{n}\cdot\boldsymbol{n} - \left(p - \frac{J^2}{\rho^{v}}\right) = \psi^{\mathrm{x}}K + (\nabla_s\cdot(2\alpha\mathbb{D} + \lambda(\mathrm{tr}\,\mathbb{D})\mathbb{P}))\cdot\boldsymbol{n}, \tag{5.1c}$$

$$\boldsymbol{S}\boldsymbol{n}\cdot\boldsymbol{t} = (-\mu_s\nabla_s n^{\mathrm{x}} - \eta_s^{\mathrm{x}}\nabla_s\theta + \nabla_s\cdot(2\alpha\mathbb{D} + \lambda(\mathrm{tr}\,\mathbb{D})\mathbb{P}))\cdot\boldsymbol{t}, \tag{5.1d}$$

$$\beta_s V^{mig} = -l\left(\frac{\theta}{\theta_s} - 1\right) - \left(p - \frac{J^2}{\rho^{v}}\right) - \psi_s\left(\frac{n}{n_s} - 1\right) + \tfrac{1}{2}\rho|\boldsymbol{u}|^2, \tag{5.1e}$$

$$\mathring{n}^{\mathrm{x}} + n^{\mathrm{x}}(\nabla_s\cdot\boldsymbol{u}_s - KV) = \kappa_n^{\mathrm{x}}\nabla_s\cdot(\nabla_s n^{\mathrm{x}}) - \kappa_n(\nabla n)\cdot\boldsymbol{n} - nV^{mig}. \tag{5.1f}$$

Here, $\alpha > 0$ and $\alpha + \lambda > 0$ are the interfacial shear and dilatational viscosities. Also, ψ_s and n_s are the saturation values of the bulk free-energy density of the solution and the bulk molecular density. The time derivative $\mathring{n}^{\mathrm{x}}$ accounts for the surface molecular density change at the interface $z = h(x, t)$: given a normally constant extension of a surface field φ (Cermelli, Fried & Gurtin 2005), $\mathring{\varphi}$ can be related to the spatial time-rate of φ via $\mathring{\varphi} = \varphi_t + \boldsymbol{u}_s\cdot\nabla_s\varphi$. Also, $\mathbb{D}$ denotes the interfacial rate-of-stretch as defined in terms of the interfacial limit of the bulk rate-of-stretch $\boldsymbol{D}$ and the interfacial projector $\mathbb{P} = \boldsymbol{1} - \boldsymbol{n}\boldsymbol{n}$, by

$$\mathbb{D} = \mathbb{P}\boldsymbol{D}\mathbb{P}.$$

In the presence of a surfactant, the dependence of the disjoining pressure on the bulk and interfacial surfactant molecular densities n and n^{x} of the surfactant is trivial. Following Danov *et al.* (1998), we assume that the disjoining pressure term $A/6\pi h^3$ depends on n and n^{x} only through the Hamaker constant A. This simplifying assumption may not generally hold. Performing self-consistent field calculations, theoretical estimates of the Hamaker constant A can be obtained on the basis of a multilayer film model (Müller *et al.* 2001). Following this approach, Gokhale, Plawsky & Waymer (2005) determined the Hamaker constant A for a solution of Silwet L-77 in DI water in good agreement with experimental data. These authors also found that a disjoining pressure model based on the representation $A/6\pi h^3$, with the Hamaker constant A estimated by this fashion, is applicable at film thicknesses of the order of a few nanometres. This motivates the use of the disjoining pressure of this form appearing in (5.1*c*).

The right-hand sides of the normal and tangential momentum balances (5.1*c*) and (5.1*d*) acquire additional terms accounting for the influence of the surface viscosity. The right-hand side of the configurational momentum balance (5.1*e*) acquires the term $-\psi_s(n/n_s - 1)$, showing an explicit dependence on the molecular density. Besides that, the system involves the additional equation, (5.1*f*), describing the balance between the bulk and surface molecular densities. We scale the bulk molecular density n, the surface molecular density n^{x}, and the chemical potential according to

$$\tilde{n} = \frac{n}{n_s}, \qquad \tilde{n}^{\mathrm{x}} = \frac{n^{\mathrm{x}}}{n_s^{\mathrm{x}}}, \qquad \tilde{\mu} = \frac{\mu}{\mu_s}, \tag{5.2}$$

where n_s and n_s^{x} are the saturation values of the bulk and surface molecular densities, respectively. This gives rise to the following additional dimensionless parameters:

$$A_3 = \frac{\psi_s\theta_s}{l\Delta\theta}, \quad M_n = \frac{h_0\mu_s n_s^{\mathrm{x}}c}{2\kappa\nu}, \quad P_n = \frac{\nu}{\kappa_n}, \quad P_{n^{\mathrm{x}}} = \frac{h_0\nu}{\kappa_n^{\mathrm{x}}}, \quad b = \frac{n_s h_0}{n_s^{\mathrm{x}}}, \quad \Omega = \frac{\xi}{2\rho\nu h_0}. \tag{5.3}$$

Variable	Units	Value
η_s^{x}	$\mathrm{N\,m^{-1}\,K^{-1}}$	4.3×10^{-4}
ψ_s^{x}	$\mathrm{N\,m^{-1}}$	1.9
ψ_s	$\mathrm{J\,mol^{-1}}$	10^{-3}
n_s^{x}	$\mathrm{mol\,m^{-2}}$	1.3×10^{-5}
n_s	$\mathrm{mol\,m^{-3}}$	0.1
ξ	m Pa s	10^{-6}
n_∞	$\mathrm{mol\,m^{-3}}$	10^{-1}
μ_s	$\mathrm{J\,mol^{-1}}$	10^{3}
κ_n	$\mathrm{m^2\,s^{-1}}$	4.3×10^{-8}
$\kappa_{n^{\mathrm{x}}}$	$\mathrm{m^2\,s^{-1}}$	1.7×10^{-8}

TABLE 4. Material properties. The values of η_s^{x}, ψ_s^{x}, n_s^{x}, κ_n and $\kappa_{n^{\mathrm{x}}}$ for sulfur in the molten iron are taken from Winkler & Amberg (2005); the values of n_s, ξ and n_∞ are taken from Danov *et al.* (1998). Estimates for ψ_s and μ_s are made on the basis of data provided by Tanaka & Gubbins (1992).

Parameter	Value
A_3	1.8×10^{-4}
M	5.7×10^{-4}
M_n	8.6×10^{-3}
N	0.1
P_n	4.6
$P_{n^{\mathrm{x}}}$	1.2×10^{-7}
b	10^{-4}
Ω	3×10^{6}
Σ	633

TABLE 5. Dimensionless parameters at $h_0 = 100\,\text{Å}$ and $\Delta\theta = 2\,\mathrm{K}$.

Here, A_3 is the surfactant activity; M_n is molecular density Marangoni number; P_n and $P_{n^{\mathrm{x}}}$ are bulk and surface molecular density Prandtl numbers; b is the ratio of the bulk and the interface saturation concentrations; and Ω is the dimensionless interfacial viscosity. κ_n, κ_n^{x} and ξ are the surfactant bulk diffusivity, the surfactant interface diffusivity, and the interfacial viscosity, respectively. We failed to find parameters values for surfactants in molten sodium. For of η_s^{x}, ψ_s^{x}, n_s^{x}, κ_n and $\kappa_{n^{\mathrm{x}}}$, we used values for sulfur in molten iron provided by Winkler & Amberg (2005). For n_s, ξ and n_∞, we used values provided by Danov *et al.* (1998). Finally, we estimated ψ_s and μ_s on the basis of data provided by Tanaka & Gubbins (1992). The parameter values are collected in table 4 and the associated dimensionless numbers resulting for $h_0 = 100\,\text{Å}$ and $\Delta\theta = 2$, are given in table 5.

When the surfactant is present, the system of dimensionless equations (2.7)–(2.8) governing the dynamics of liquid should be complemented with the equation for the transfer of the bulk molecular density n. In dimensionless form, the bulk transport equation is

$$P_n \frac{\mathrm{D}n}{\mathrm{D}t} = \nabla^2 n.$$

On the substrate, we require that $\partial n/\partial z = 0$. On the liquid–vapour interface, we impose the conditions representing the dimensionless counterparts to (5.1). To close the system of equations, we must add the sorption isotherm relating n^{x} and n.

Following the approach of Jensen & Grotberg (1993) and looking for the molecular density solution in the form $n(x,z,t)=n^0(x,t)+\epsilon^2 n^1(x,z,t)$ (where ϵ is an appropriate small parameter), we find that, to the leading order, the solution to the system describing the evolution of the thin film with the surfactant splits into two subsystems. The first subsystem, which determines how u, w and θ depend on z, has the form

$$u(z)=\frac{p_x}{2}z(z-h)+\frac{\mathscr{V}}{h}z, \tag{5.4a}$$

$$w(z)=-\frac{p_{xx}}{2}\left(\frac{z^3}{3}-\frac{hz^2}{2}\right)+\frac{p_x}{4}z^2h_x-\left(\frac{\mathscr{V}z^2}{2h}\right)_x, \tag{5.4b}$$

$$\theta(z)=1+\left(A_1J-1+A_2\left(\Sigma h_{xx}-\frac{\Pi}{h^3}\right)-A_3(n-1)\right)\frac{z}{h}. \tag{5.4c}$$

From (5.4), knowledge of p, h, $\mathscr{V}$, J and n is sufficient to determine u, w and θ. The second subsystem determines the long-wave evolution of the system and has the form

$$p=E^2D^{-1}J^2+\frac{\Pi}{h^3}-\Sigma h_{xx} \tag{5.5a}$$

$$EJ=-h_t+\tfrac{1}{12}(p_xh^3)_x-\tfrac{1}{2}(\mathscr{V}h)_x, \tag{5.5b}$$

$$N\mathscr{V}_x=\left(1-A_1J-A_2\left(\Sigma h_{xx}-\frac{\Pi}{h^3}\right)+A_3(n-1)\right)\frac{1}{h}-J, \tag{5.5c}$$

$$\frac{p_xh}{2}+\frac{\mathscr{V}}{h}+\frac{2M_n}{Pr}n^{\mathrm{x}}_x+\frac{2M}{Pr}\left(A_1J_x+A_2\left(\Sigma h_{xxx}+\frac{3\Pi h_x}{h^4}\right)-A_3n_x\right)$$
$$=2\Omega\left(\mathscr{V}_{xx}n^{\mathrm{x}}+\mathscr{V}_xn^{\mathrm{x}}_x\right), \tag{5.5d}$$

$$(n^{\mathrm{x}}+bHn)_t+\left(\mathscr{V}n^{\mathrm{x}}-\frac{b}{P_{n^{\mathrm{x}}}}n^{\mathrm{x}}_x-bn\left(\frac{p_xh^3}{12}-\frac{\mathscr{V}h}{2}\right)-\frac{bhn_x}{P_n}\right)_x=0, \tag{5.5e}$$

$$n^{\mathrm{x}}=\frac{n}{n+n_\infty}. \tag{5.5f}$$

Equation (5.5f) represents the dimensionless sorption isotherm, where n_∞ is the reference value of n. To investigate the stability of system (5.5), we perturb the time-dependent base state, as characterized by $\hat{h}$, $\hat{J}$, $\hat{p}$, $\hat{n}$, $\hat{n}^{\mathrm{x}}$, and obtain a system

$$\dot{H}(t)=F[H(t),n(t)],\qquad \dot{n}(t)=G[H(t),n(t)], \tag{5.6}$$

of linear equations for the surface shape and the molecular density perturbation amplitudes.

5.1. *Base state*

In addition to the equations (3.3), the base state includes the condition $(\hat{n}^{\mathrm{x}}+b\hat{n}\hat{h})_t=0$ imposing surfactant balance in the film (Danov *et al.* 1998). The leading-order solutions for variables $\hat{J}$, $\hat{\theta}$, $\hat{p}$ retain the form given by (3.6b–d), but the film thickness and the surface molecular density become:

$$\hat{h}_t=-\frac{1+A_2\Pi/\hat{h}(t)^3+A_3(\hat{n}-1)}{A_1+\hat{h}(t)}E, \tag{5.7a}$$

$$\hat{n}^{\mathrm{x}}(t)=\frac{1}{2}\left(1+\Lambda+bn_\infty\hat{h}(t)-\sqrt{(bn_\infty\hat{h}(t)+1+\Lambda)^2-4\Lambda}\right), \tag{5.7b}$$

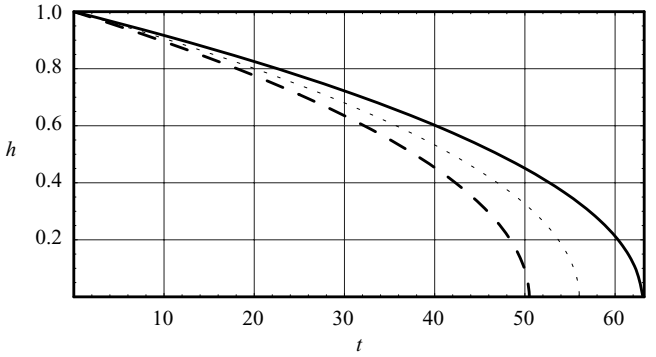

FIGURE 8. Film thickness evolution for different A_3: $A_3 = 0$ (dashed line), $A_3 = 0.1$ (dotted line), $A_3 = 0.2$ (solid line). Other parameters were taken as $A_1 = 0.005$, $A_2 = 0$, $E = 0.01$, $b = 0.001$, $n^{\mathrm{x}} = 0.1$, $n_\infty = 0.1$.

where $\Lambda = \hat{n}^{\mathrm{x}}(0) + b\hat{h}(0)\hat{n}(0)$ is a constant defined by the initial values at $t = 0$. Note that the energy flux characterized by N does not affect the base state (5.7).

Equation (5.7*a*) for the evolution of the film thickness explicitly includes the influence of the surfactant activity A_3. The actual value of A_3 is usually small (table 5). To obtain a qualitative understanding of the effect of the surfactant on the evolution of the base state, we therefore used much larger values of A_3. Figure 8 shows the increase of the disappearance time t_d (when $h = 0$, in the case when the liquid partially wets the substrate) as the surfactant activity A_3 increases. In the case when the liquid completely wets the substrate, the stationary state corresponding to the layer adsorbed by the substrate is

$$h^* = \left(\frac{-A_3 \Pi}{1 + A_2/(n^{\mathrm{x}^*} - 1)} \right)^{1/3}.$$

5.2. *Stability*

To study the influence of the energy flux and the effective pressure, we limit the stability analysis to the simple case of a quasi-static base state. Taking the base state $\hat{h} = 1$ and $\hat{n} = \hat{n}(0)$ and assuming that $H \sim \mathrm{e}^{\omega t}$ and $n \sim \mathrm{e}^{\omega t}$, we obtain a dispersion relation of the form

$$\omega = \omega(k, A_1, A_2, A_3, D, E, M, M_n, Pr, P_n, P_{n^{\mathrm{x}}}, N, \Pi, \Sigma, b, \Omega).$$

Because of the small value of A_3, we did not observe a significant influence of this parameter on the film stability. The influence of the coefficient A_2 associated with the effective pressure on the stability of the film with the surfactant is shown in figure 9(*a*). The solid line shows the dispersion curve for $A_2 = 0.05$ and the dashed line shows the case $A_2 = 0$. This result is qualitatively the same as for the case of the surfactant-free film (figure 4*b*). Increasing A_2 exerts a stabilizing influence on the system. Also, we see that with surfactant, shown in figure 9(*a*) (the initial surface molecular density $n^{\mathrm{x}} = 0.1$), the growth rate ω is substantially lower than that for the surfactant-free case $n^{\mathrm{x}} = n = 0$ shown in figure 4(*b*). This indicates the stabilizing influence of the surfactant. The influence of the effective pressure (difference between the solid and the dashed lines) was found to be appreciable for all investigated values of the initial surface molecular density $n^{\mathrm{x}}(0)$ and other parameters corresponding to molten metals.

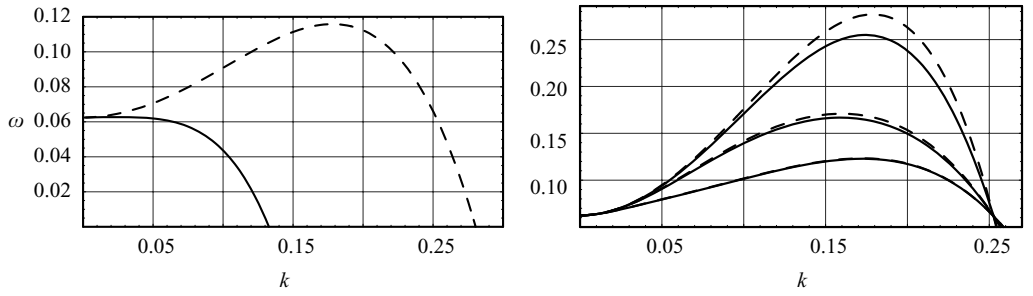

FIGURE 9. Change in the dispersion curve due to the change of (*a*) the effective pressure A_2 ($N=0$): $A_2=0$ (dashed curve), $A_2=0.05$ (solid curve). The initial surface molecular density $n^{\mathrm{x}}=0.1$. (*b*) the interfacial energy flux N ($A_2=0$): $N=0$ (dashed curve), $N=0.1$ (solid curve). Three pairs correspond to the initial surface molecular density $n^{\mathrm{x}}=0$, $n^{\mathrm{x}}=10^{-4}$, and $n^{\mathrm{x}}=10^{-3}$.

Figure 9(*b*) shows the influence of the interfacial energy flux (difference between the solid and the dashed lines) for $n^{\mathrm{x}}(0)=0$ (upper pair of curves), $n^{\mathrm{x}}(0)=10^{-4}$ (middle pair of curves), and $n^{\mathrm{x}}(0)=10^{-3}$ (lower pair of curves). The solid lines show the dispersion curve for $N=0.1$ and the dashed lines show the case $N=0$. Aside from the stabilizing influence of the surfactant, we see that as n^{x} grows, the dashed and solid curves approach one another, indicating a decreasing influence of the parameter N on the stability. At $n^{\mathrm{x}}=10^{-3}$, the curves almost merge, indicating the negligible influence of N. An explanation might be found in the fact that the interfacial viscosity and, hence, the dissipation, increases with n^{x}. Energy transport along the interface therefore slows with increasing n^{x}.

The calculations of this section demonstrate that the influence of the effective pressure (difference between the dashed and the solid lines in figure 9*a*), governed by A_2, on the stability of the thin film remains significant even in the presence of the surfactant. However, the results presented in figure 9(*b*) indicate that increasing the amount of surfactant suppresses the energy flux along the interface, governed by N.

6. Summary

An analysis of the linear stability of the evaporating thin liquid film has been performed. The model used in our analysis accounts for: (i) the influence of the energy flux along the film surface; (ii) the influence of the effective pressure accounting for vapour recoil. The results reveal conditions under which these two effects are important. We find that these effects have a small influence for liquids like water and ethanol, for which the evaporation number E is small. The effects turn out to be appreciable for liquids with relatively large ($E\sim 0.1$) evaporation numbers and with small ($Pr\ll 1$) Prandtl numbers. In particular, we show that, for molten metals such as sodium, a consideration of the effective pressure substantially affects the values of growth rate and cutoff wavenumbers. When the interfacial energy transport and effective pressure are negligible, our model reduces to that of Burelbach *et al.* (1988) and, at $N=A_2=0$, we recover their results.

We observe the stabilizing influences of the effective pressure for parameter values corresponding to molten metals. This result follows from the fact that this effect arises from additional dissipative mechanisms associated with the corresponding terms (Fried *et al.* 2006). Specifically, we demonstrate that consideration of the effective pressure makes it possible to observe the influence of the van der Waals

interaction on the film evolution close to the instant of rupture. The analysis of the base state shows that, for a liquid partially wetting the substrate, the disjoining pressure shortens the evolution time of the evaporating film – the thickness of which changes from the initial value to zero. When the liquid completely wets the substrate, rupture does not occur and the film evolves into the stationary state representing a thin liquid layer adsorbed onto the substrate. This result for a thin film is similar to that obtained by Moosman & Homsy (1980) for an evaporating meniscus. The expression for the thickness of the adsorbed layer obtained in our work agrees with the estimate obtained by Wayner (1999). Thus, we demonstrate that the presence of the effective pressure removes the degeneracy of the evolution of the base state with respect to the cases when a liquid partially or completely wets the substrate.

Calculations by Burelbach *et al.* (1988) revealed limitations of the lubrication approximation near the disappearance time t_d. At t_d, when the thickness h vanishes, the vertical velocity becomes large according to $h_t \sim 1/(A_1 + h)$ (if $A_1 = 0$), which contradicts the lubrication approximation. The results of our analysis show that (i) the change in the film thickness h is always singular and follows $h_t \sim A_2\Pi/(A_1+h)h^3$ for small h, even for the case $A_1 \neq 0$; (ii) the change in the film thickness h occurs even faster than predicted by Burelbach *et al.* (1988). This reflects the influence of the disjoining pressure.

The thin-film rupture times calculated by Williams & Davis (1982) and Yiantsios & Higgins (1991) by means of linear and nonlinear theories are of the same order of magnitude. Even though the rupture time determined by nonlinear theory is shorter than that obtained by linear analysis, they give qualitatively the same estimates. For this reason, we leave investigation of the influence of the energy flux on the surface and the effective pressure on the nonlinear evolution of thin film for later consideration.

Our calculations also show that, whereas the presence of a non-volatile dissolved surfactant on the film interface suppresses the energy flux along the surface, the effective pressure remains an important factor affecting film stability.

This work was supported by DOE. We thank V. Ajaev, X. Chen, S. Davis, G. Homsy, M. Miksis and A. Shen for helpful discussions.

Appendix. Long-wave approximation

Here we provide some details of how the boundary conditions (2.7) and (2.8) can be reduced to (2.9)–(2.11). We adopt a rectangular Cartesian basis $\{\boldsymbol{e}_1, \boldsymbol{e}_3\}$, where the outward normal $\boldsymbol{n}$, tangent vector $\boldsymbol{t}$ to the surface, curvature K, and velocity are given by

$$\boldsymbol{n} = \frac{-h_x\boldsymbol{e}_1 + \boldsymbol{e}_3}{\left(1+h_x^2\right)^{1/2}}, \qquad \boldsymbol{t} = \frac{\boldsymbol{e}_1 + h_x\boldsymbol{e}_3}{\left(1+h_x^2\right)^{1/2}}, \qquad K = \frac{h_{xx}}{\left(1+h_x^2\right)^{3/2}}, \qquad \boldsymbol{u} = u\boldsymbol{e}_1 + w\boldsymbol{e}_3,$$

with h_x denoting the derivative of h with respect to the horizontal coordinate x. Taking into consideration that

$$\frac{\mathrm{D}h}{\mathrm{D}t} = h_x u^i + h_t = w^i$$

(where the superscript 'i' indicates the interface), we find expressions for the normal velocity V, the migrational velocity V^{mig}, and the product KV of curvature and

normal velocity as

$$V = \boldsymbol{u}^i \cdot \boldsymbol{n} = \frac{-h_x u^i + w^i}{\left(1+h_x^2\right)^{1/2}} = \frac{h_t}{\left(1+h_x^2\right)^{1/2}}, \tag{A.1a}$$

$$V^{mig} = V - \boldsymbol{u}\cdot\boldsymbol{n} = \frac{h_x u - w + h_t}{\left(1+h_x^2\right)^{1/2}}, \tag{A.1b}$$

$$KV = \frac{h_t h_{xx}}{\left(1+h_x^2\right)^2}. \tag{A.1c}$$

Assuming that the horizontal scale of the liquid motion is significantly larger than the vertical one and that the time evolution is slow enough, we apply a long-wave approximation. Following Williams & Davis (1982), we take the dimensionless wavenumber k to be a small parameter. According to this choice, we apply the change of variables

$$x = \frac{X}{k}, \quad z = Z, \quad t = \frac{T}{k},$$

and expand all variables in powers of k:

$$u = U + kU_1 + \cdots, \qquad w = k(W + kW_1 + \cdots), \qquad p = k^{-1}(P + kP_1 + \cdots),$$
$$\theta = \Theta + k\theta_1 + \cdots, \qquad J = J + kJ_1 + \cdots.$$

Here, u, w, p, θ, J and h are functions of variables x, z and t, whereas their long-wave counterparts U, W, P, Θ, J and H are functions of X, Z and T. To the leading order, the normal, tangent vectors and the curvature are

$$\boldsymbol{n} = -kH_X\boldsymbol{e}_1 + \boldsymbol{e}_3 + o(k), \tag{A.2a}$$

$$\boldsymbol{t} = \boldsymbol{e}_1 + kH_X\boldsymbol{e}_3 + o(k), \tag{A.2b}$$

$$K = k^2 H_{XX} + o(k^2). \tag{A.2c}$$

Using these expressions, we calculate gradients of the normal and tangent vectors, projector $\mathbb{P}$, bulk rate of stretch $\boldsymbol{D}$ and surface velocity $\boldsymbol{u}_s$ as

$$\nabla\boldsymbol{n} = -k^2 H_{XX}\boldsymbol{e}_1\boldsymbol{e}_1 - k^3 H_X H_{XX}\boldsymbol{e}_3\boldsymbol{e}_1 + o(k^3), \tag{A.3a}$$

$$\nabla\boldsymbol{t} = -k^3 H_X H_{XX}\boldsymbol{e}_1\boldsymbol{e}_1 + k^2 H_{XX}\boldsymbol{e}_3\boldsymbol{e}_1 + o(k^3), \tag{A.3b}$$

$$\mathbb{P} = \boldsymbol{e}_1\boldsymbol{e}_1 + kH_X\boldsymbol{e}_1\boldsymbol{e}_3 + kH_X\boldsymbol{e}_3\boldsymbol{e}_1 + o(k), \tag{A.3c}$$

$$\boldsymbol{D} = \tfrac{1}{2}(2kU_X\boldsymbol{e}_1\boldsymbol{e}_1 + (U_Z + k^2W_X)\boldsymbol{e}_1\boldsymbol{e}_3 + (U_Z + k^2W_X)\boldsymbol{e}_3\boldsymbol{e}_1 + 2kW_Z\boldsymbol{e}_3\boldsymbol{e}_3) + o(k^2), \tag{A.3d}$$

$$\boldsymbol{u}_s = \mathbb{P}\boldsymbol{u} = \left(U + k^2\left(H_X W - H_X^2 U\right)\right)\boldsymbol{e}_1 + kH_X U\boldsymbol{e}_3 + o(k^2). \tag{A.3e}$$

Now, we obtain a leading-order estimate of the terms KV and $\nabla_s\cdot\boldsymbol{u}_s$ entering the equation (2.8b); the surface rate of stretch $\mathbb{D}$, the projections of $\boldsymbol{Dn}$ onto the directions $\boldsymbol{n}$ and $\boldsymbol{t}$ entering the equations (2.8c, d):

$$KV = k^3 H_T H_{XX} + o(k^3), \tag{A.4a}$$

$$\nabla_s\cdot\boldsymbol{u}_s = \mathbb{P} : \nabla\boldsymbol{u}_s = k(U_X + H_X U_Z) + o(k), \tag{A.4b}$$

$$\mathbb{D} = \mathbb{P}\boldsymbol{D}\mathbb{P} = k(U_X + H_X U_Z)\boldsymbol{e}_1\boldsymbol{e}_1 + k^2 H_X(U_X + H_X U_Z)\boldsymbol{e}_1\boldsymbol{e}_3 + k^2 H_X(U_X + H_X U_Z)\boldsymbol{e}_3\boldsymbol{e}_1 + o(k^2), \tag{A.4c}$$

$$2\boldsymbol{Dn}\cdot\boldsymbol{n} = -2k(U_X + U_Z h_X) + o(k^2), \tag{A.4d}$$

$$2\boldsymbol{Dn}\cdot\boldsymbol{t} = U_Z + o(k). \tag{A.4e}$$

To calculate the projection of the surface divergence $\nabla_s \cdot (2\bar{\alpha}\mathbb{D} + \bar{\lambda}(\mathrm{tr}\,\mathbb{D})\mathbb{P})$ onto the normal direction in the momentum balance equation (5.1*c*) we note that

$$\boldsymbol{n} \cdot (\nabla_s \cdot (2\bar{\alpha}\mathbb{D} + \bar{\lambda}(\mathrm{tr}\,\mathbb{D})\mathbb{P})) = \mathbb{P} : \nabla((2\bar{\alpha}\mathbb{D} + \bar{\lambda}(\mathrm{tr}\,\mathbb{D})\mathbb{P})^{\top}\boldsymbol{n}) - (2\bar{\alpha}\mathbb{D} + \bar{\lambda}(\mathrm{tr}\,\mathbb{D})\mathbb{P}) : \nabla\boldsymbol{n}.$$

Since $(2\bar{\alpha}\mathbb{D} + \bar{\lambda}(\mathrm{tr}\,\mathbb{D})\mathbb{P})^{\top}\boldsymbol{n} = \boldsymbol{0}$, we need only calculate the second term, which is

$$2\bar{\alpha}\mathbb{D} + \bar{\lambda}(\mathrm{tr}\,\mathbb{D})\mathbb{P} = (2\bar{\alpha} + \bar{\lambda})k(U_X + H_X U_Z)\boldsymbol{e}_1\boldsymbol{e}_1 + o(k).$$

Using the expression (A.2*e*) for the $\nabla\boldsymbol{n}$ we obtain

$$(2\bar{\alpha}\mathbb{D} + \bar{\lambda}(\mathrm{tr}\,\mathbb{D})\mathbb{P}) : \nabla\boldsymbol{n} = o(k^2),$$

which gives the projection of the surface divergence onto the normal direction

$$\boldsymbol{n} \cdot (\nabla_s \cdot (2\bar{\alpha}\mathbb{D} + \bar{\lambda}(\mathrm{tr}\,\mathbb{D})\mathbb{P})) = o(k^2). \tag{A.5}$$

To the leading order, this term does not contribute in the normal component of the momentum balance equation (5.1*c*). The tangential component of the surface divergence entering equation (5.1*d*), is

$$\boldsymbol{t} \cdot (\nabla_s \cdot (2\bar{\alpha}\mathbb{D} + \bar{\lambda}(\mathrm{tr}\,\mathbb{D})\mathbb{P})) = \mathbb{P} : \nabla((2\bar{\alpha}\mathbb{D} + \bar{\lambda}(\mathrm{tr}\,\mathbb{D})\mathbb{P})^{\top}\boldsymbol{t}) - (2\bar{\alpha}\mathbb{D} + \bar{\lambda}(\mathrm{tr}\,\mathbb{D})\mathbb{P}) : \nabla\boldsymbol{t}. \tag{A.6}$$

Direct calculation shows that,

$$(2\bar{\alpha}\mathbb{D} + \bar{\lambda}(\mathrm{tr}\,\mathbb{D})\mathbb{P})^{\top}\boldsymbol{t} = \xi n^{\mathrm{x}} k(U_X + H_X U_Z)\boldsymbol{e}_1 + o(k), \tag{A.7a}$$

$$(2\bar{\alpha}\mathbb{D} + \bar{\lambda}(\mathrm{tr}\,\mathbb{D})\mathbb{P}) : \nabla\boldsymbol{t} = o(k^4). \tag{A.7b}$$

In the expressions (A.7), we follow Danov *et al.* (1998) and assume that the interfacial viscosity $2\alpha + \lambda$ arises only due to the presence of the surfactant n^{x} on the surface and is therefore $2\alpha + \lambda = \xi n^{\mathrm{x}}$. Calculation of the first term on the right-hand side of (A.6) gives

$$\begin{aligned}\mathbb{P} : \nabla((2\bar{\alpha}\mathbb{D} + \bar{\lambda}(\mathrm{tr}\,\mathbb{D})\mathbb{P})^{\top}\boldsymbol{t}) &= k^2\xi\, n^{\mathrm{x}}_X(U_X + H_X U_Z) \\ &+ \xi\, n^{\mathrm{x}} k^2\,[(U_{XX} + H_{XX}U_Z + H_X U_{ZX}) + H_X(U_{XZ} + H_X U_{ZZ})] + o(k^2).\end{aligned} \tag{A.8}$$

Using the explicit expression (2.12*a*) for the velocity component U, we can calculate the following identities

$$U_X + H_X U_Z = \mathscr{V}_X,$$
$$U_{XX} + H_{XX}U_Z + 2H_X U_{ZX} + H_X^2 U_{ZZ} = \mathscr{V}_{XX}.$$

Finally, we obtain the tangential component of the surface divergence in equation (5.1*d*) as

$$\boldsymbol{t} \cdot (\nabla_s \cdot (2\bar{\alpha}\mathbb{D} + \bar{\lambda}(\mathrm{tr}\,\mathbb{D})\mathbb{P})) = k^2\xi\left(\mathscr{V}_{XX}n^{\mathrm{x}} + \mathscr{V}_X n^{\mathrm{x}}_X\right) + o(k^2). \tag{A.9}$$

Note that, in the surfactant-free case $n^{\mathrm{x}} = 0$ and

$$\boldsymbol{t} \cdot (\nabla_s \cdot (2\bar{\alpha}\mathbb{D} + \bar{\lambda}(\mathrm{tr}\,\mathbb{D})\mathbb{P})) = 0.$$

To the leading order, the governing equations become

$$-P_X + U_{ZZ} = 0, \tag{A.10a}$$

$$-P_Z = 0, \tag{A.10b}$$

$$\Theta_{ZZ} = 0, \tag{A.10c}$$

$$U_X + W_Z = 0; \tag{A.10d}$$

the boundary conditions (2.7) reduce to

$$W = 0, \quad U = 0, \quad \Theta = 1; \tag{A.11}$$

further using the equations (A.4), we can now rewrite the boundary conditions on liquid–vapour interface (2.8) as

$$E(J + kJ_1) = k(-h_T - h_X U + W), \tag{A.12a}$$

$$kN\mathscr{V}_X = -\Theta_Z - J, \tag{A.12b}$$

$$\frac{k\Pi}{h^3} - P - 2k^2\mathscr{V}_X = -kE^2D^{-1}J^2 + k^3\Sigma h_{XX}(1 - C\Theta), \tag{A.12c}$$

$$-\frac{1}{2}U_Z = kMPr^{-1}(\Theta_X + h_X\Theta_Z), \tag{A.12d}$$

$$A_1 J = \Theta + A_2\left(\frac{P}{k} - \tfrac{1}{2}(U^2 + k^2W^2) - E^2D^{-1}J^2\right). \tag{A.12e}$$

To retain the physical effects important for our analysis, we adopt the scales

$$E = k\bar{E}, \quad D = k^3\bar{D}, \quad A_1 = \bar{A}_1, \quad A_2 = k\bar{A}_2,$$
$$N = \frac{\bar{N}}{k}, \quad M = \frac{\bar{M}}{k}, \quad \Omega = \frac{\bar{\Omega}}{k^2}, \quad \Pi = \frac{\bar{\Pi}}{k}, \quad \Sigma = \frac{\bar{\Sigma}}{k^3},$$

where the quantities with superposed bars are assumed to be of the order of $O(1)$ as $k \to 0$. Finally, noting that

$$k^3\Sigma(1 - C\theta) = \bar{\Sigma} - k^2\bar{M}Pr^{-1}\theta = \bar{\Sigma} + O(k^2),$$

we may reduce the system (A.12) to

$$\bar{E}J = -h_T - h_X U + W, \tag{A.13a}$$

$$\bar{N}\mathscr{V}_X = -\Theta_Z - J, \tag{A.13b}$$

$$\frac{\bar{\Pi}}{h^3} - P = -\bar{E}^2\bar{D}^{-1}J^2 + \bar{\Sigma}h_{XX}, \tag{A.13c}$$

$$-\frac{1}{2}U_Z = \bar{M}Pr^{-1}(\Theta_X + h_X\Theta_Z), \tag{A.13d}$$

$$A_1 J = \Theta + \bar{A}_2(P - \bar{E}^2\bar{D}^{-1}J^2). \tag{A.13e}$$

REFERENCES

Ajaev, V. S. & Homsy, G. M. 2001 Steady vapor bubbles in rectangular microchannels. *J. Colloid Interface Sci.* **240**, 259–271.

Burelbach, J. P., Bankoff, S. G. & Davis, S. H. 1988 Nonlinear stability of evaporating/condensing liquid-films. *J. Fluid Mech.* **195**, 463–494.

Cammenga, H. K. 1980 Evaporation mechanisms of fluids. *In Current Topics in Materials Science* (ed. E. Kaldis), vol. 5, pp. 335–446. North-Holland.

Cermelli, P., Fried, E. & Gurtin, M. E. 2005 Transport relations for surface integrals arising in the formulation of balance laws for evolving fluid interfaces. *J. Fluid Mech.* **544**, 339–351.

Danov, K. D., Alleborn, N., Raszillier, H. & Durst, F. 1998 The stability of evaporating thin liquid films in the presence of surfactant: I. Lubrication approximation and linear analysis. *Phys. Fluids* **10**, 131–143.

Deryagin, B. V. & Churaev, N. V. 1965 Effect of film transfer upon evaporation of liquids from capillaries. *Bull. RILEM* **29**, 93–98.

Eshelby, J. D. 1951 The force on an elastic singularity. *Phil. Trans. R. Soc. Lond.* A **244**, 87–112.

Fedkin, A. V., Grossman, L. & Ghiorso, M. S. 2005 Vapor pressure and evaporation coefficient of Fe, Na and K over chondrule composition melts. In *Lunar Planetary Sci.* **36**, Abst. 2273. Lunar and Planetary Institute, Houston (CD-ROM).

Foust, O. J. 1972 *Sodium-NaK Engineering Handbook*. Gordon & Breach.

Fried, E., Gurtin, M. E. & Shen, A. Q. 2006 Theory for solvent, momentum and energy transfer between a surfactant solution and a vapor atmosphere. *Phys. Rev.* E **73**, 061601.

Gibbs, J. W. 1878 On the equilibrium of heterogeneous substances. *Trans. Connecticut Acad. Arts Sci.* **3**, 108–248.

Gokhale, J. S., Plawsky, J. L. & Wayner, P. C. 2005 Spreading, evaporation, and contact line dynamics of surfactant-laden microdrops. *Langmuir* **21**, 8188–8197.

Gurtin, M. E. 1988 Multiphase thermomechanics with interfacial structure 1. Heat conduction and the capillary balance law. *Arch. Rat. Mech. Anal.* **104**, 185–221.

Gurtin, M. E. 1995 The nature of configurational forces. *Arch. Rat. Mech. Anal.* **131**, 67–100.

Gurtin, M. E. 2000 *Configurational Forces as Basic Concepts of Continuum Physics*. Springer.

Herring, C. 1951 Surface tension as a motivation for sintering. In *The Physics of Powder Metallurgy* (ed. W. E. Kingston). McGraw-Hill.

Jain, R. K. & Ruckenstein, E. 1976 Stability of stagnant viscous film on a solid surface. *J. Colloid Interface Sci.* **54**, 108–116.

Jensen, O. E. & Grotberg, J. B. 1993 The spreading of heat or soluble surfactant along a thin liquid film. *Phys. Fluids* **5**, 58–68.

Koffman, L. D., Plesset, M. S. & Lees, L. 1984 Theory of evaporation and condensation. *Phys. Fluids* **27**, 876–880.

Moosman, S. & Homsy, G. M. 1980 Evaporating menisci of wetting fluids. *J. Colloid Interface Sci.* **73**, 212–223.

Müller, M., MacDowell, L. G., Müller-Buschbaum, P., Wunnike, O. & Stamm, M. 2001 Nano-dewetting: interplay between van der Waals- and short-ranged interactions. *J. Chem. Phys.* **115**, 9960–9969.

Oron, A., Davis, S. H. & Bankoff S. G. 1997 Long-scale evolution of thin liquid films. *Rev. Mod. Phys.* **69**, 931–980.

Palmer, H. J. 1976 The hydrodynamic stability of rapidly evaporating liquids at reduced pressure. *J. Fluid Mech.* **75**, 487–511.

Rose, J. 2000 Accurate approximate equations for intensive sub-sonic evaporation. *Intl J. Heat Mass Transfer* **43**, 3869–3875.

Schrage, W. 1953 A theoretical study of interphase mass transfer. Columbia University Press, New York.

Sheludko, A. 1967 Thin liquid films. *Adv. Colloid Interface Sci.* **1**, 391–463.

Tanaka, H. & Gubbins, K. E. 1992 Structure and thermodynamic properties of water–methanol mixtures: role of the water–water interaction. *J. Chem. Phys.* **97**, 2626–2634.

Volmer, M. 1939 *Kinetik der Phasenbildung*. T. Steinkopff, Dresden.

Wayner, P. C. 1998 Interfacial forces and phase change in thin liquid films. In *Microscale Energy Transport* (ed. Chang-Lin Tien *et al.*), pp. 187–228. Taylor & Francis.

Wayner, P. C. 1999 Intermolecular forces in phase-change heat transfer: 1998 Kern award rewiew. *AIChE J.* **45**, 2055–2067.

Wayner, P. C. 2002 Nucleation, growth and surface movement of a condensing sessile droplet. *Colloids Surf.* A **206**, 157–165.

Williams, M. B. & Davis, S. H. 1982 Nonlinear theory of film rupture. *Phys. Fluids* **90**, 220–228.

Winkler, C. & Amberg, G. 2005 Multicomponent surfactant mass transfer in GTA-welding. *Prog. Comput. Fluid Dyn.* **5**, 190–206.

Yang, H.-C., Seo, Y.-C., Kim, J.-H., Park, H.-H. & Kang, Y. 1994 Vaporization characteristics of heavy metal compounds at elevated temperatures. *Korean J. Chem. Engng* **11**, 232–238.

Yiantsios, S. G. & Higgins, B. G. 1991 Rupture of thin films: nonlinear stability analysis. *J. Colloid Interface Sci.* **147**, 341–350.